Supporting Information

pH-Dependence of the OH Reactivity of Organic Acids in the Aqueous Phase

Jessica Vejdani Amorim[1], Shuang Wu[1], Keifer Klimchuk[1], Chester Lau[1], Florence J. Williams[2], Yuanlong Huang[3], Ran Zhao[1*]

[1] Department of Chemistry, University of Alberta, 11227 Saskatchewan Drive NW, Edmonton, AB, T6G 2G2, CA.

[2] Department of Chemistry, University of Iowa, W285 Chemistry Building, Iowa City, Iowa, 52242-1294, USA.

3 Division of Chemistry and Chemical Engineering, California Institute of Technology, 1200 E California Blvd., Pasadena, CA 91125

The following content can be found in this supporting information:

Section S1. Synthesis of Pinic Acid (PA) and Limononic Acid (LA)

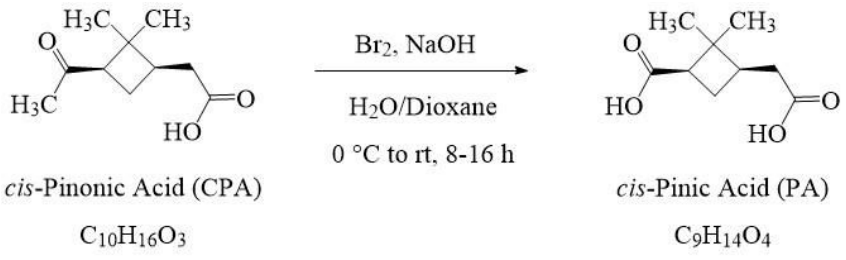

cis-Pinonic Acid (CPA) $C_{10}H_{16}O_3$

cis-Pinic Acid (PA) $C_9H_{14}O_4$

Scheme S1. Synthesis of PA.[1]

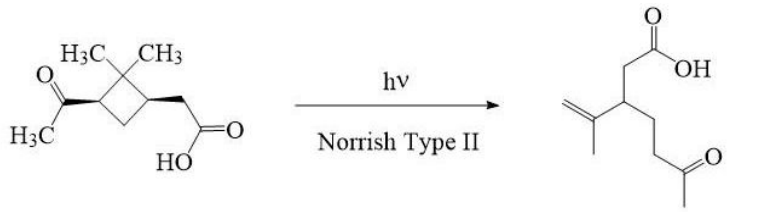

cis-Pinonic Acid (CPA) $C_{10}H_{16}O_3$

Limononic Acid (LA) $C_{10}H_{16}O_3$

Scheme S2. Synthesis of LA.

PA was synthesized via a Haloform reaction. A similar mechanism was also used in the synthesis of PA by Steimer et al.[1] When treated with bromide in basic solution, polyhalogenation and cleavage of the methyl group of CPA occurs to form PA. The structure of PA was confirmed with ^{1}H NMR and ^{13}C NMR, as presented in Fig. S1 and S2, respectively, and spectroscopic data matches literature.[2]

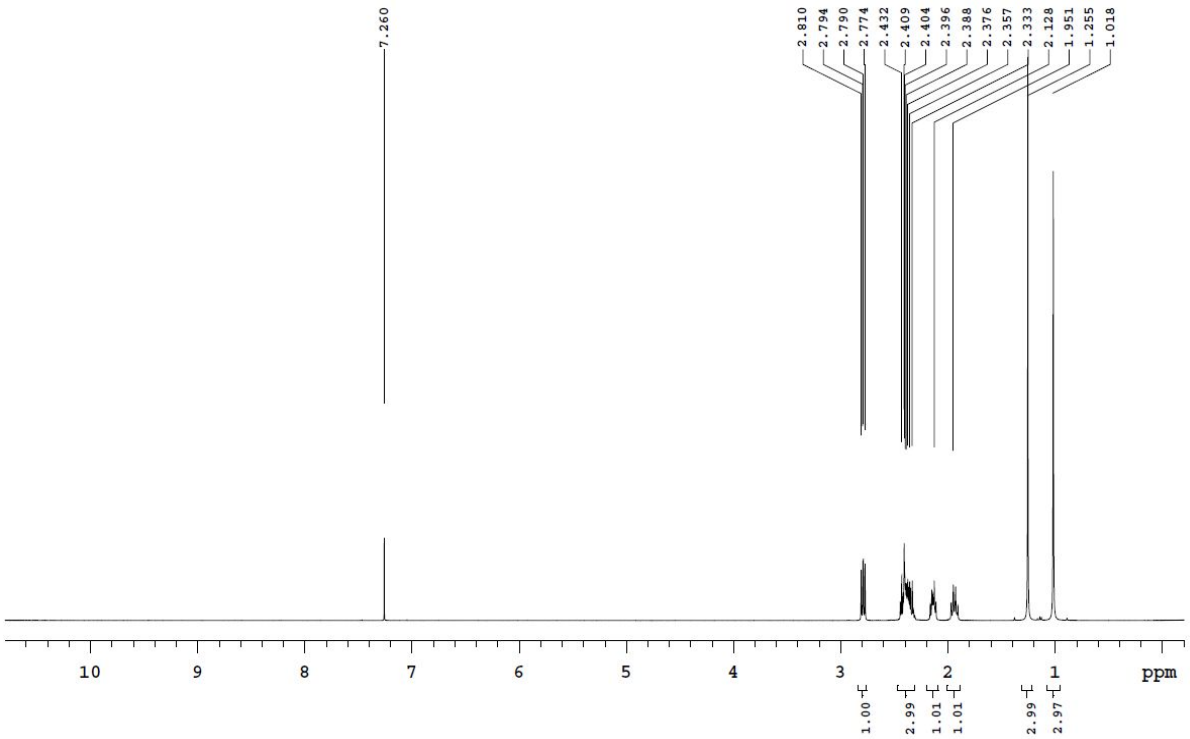

29

30 **Figure S1.** ^{1}H NMR spectrum of PA in $CDCl_3$.

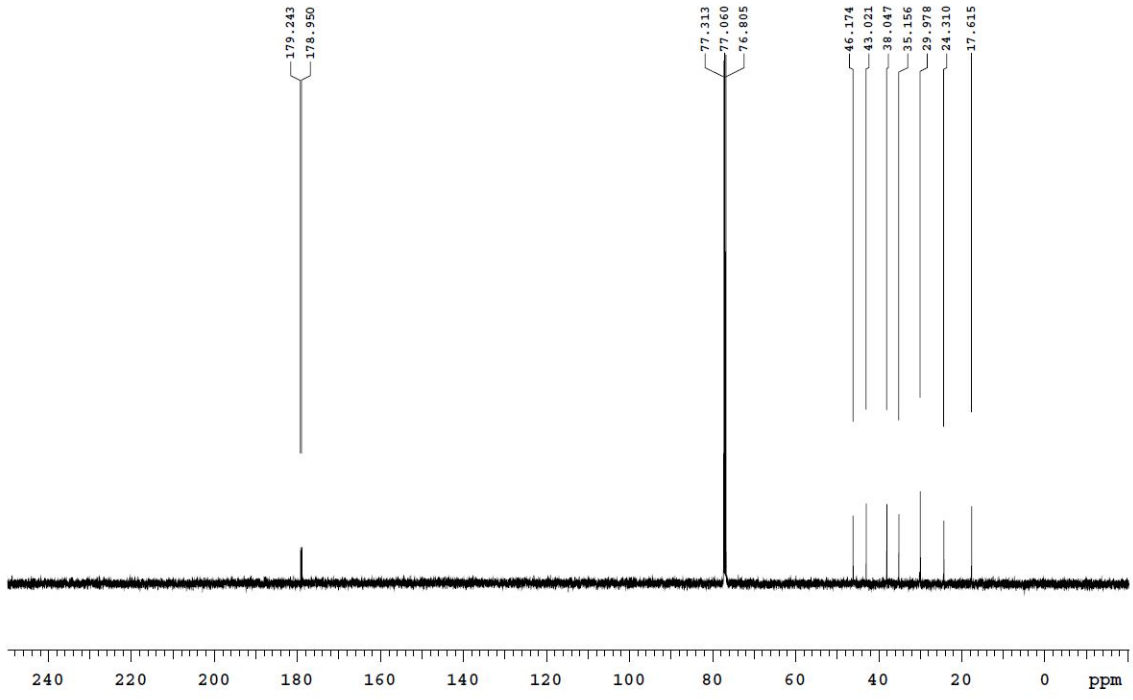

31

32 **Figure S2.** ^{13}C NMR spectrum of PA in $CDCl_3$.

LA was synthesized by exposing 150 mL of a 300 μM solution of CPA in water to UVB radiation. Aliquots were taken every 5 minutes for a total time of 25 minutes, and the reaction progress was monitored using (-)ESI-LC/MS. The decay of CPA and evolution of LA are shown in Figure S3. The synthesized LA is not further purified.

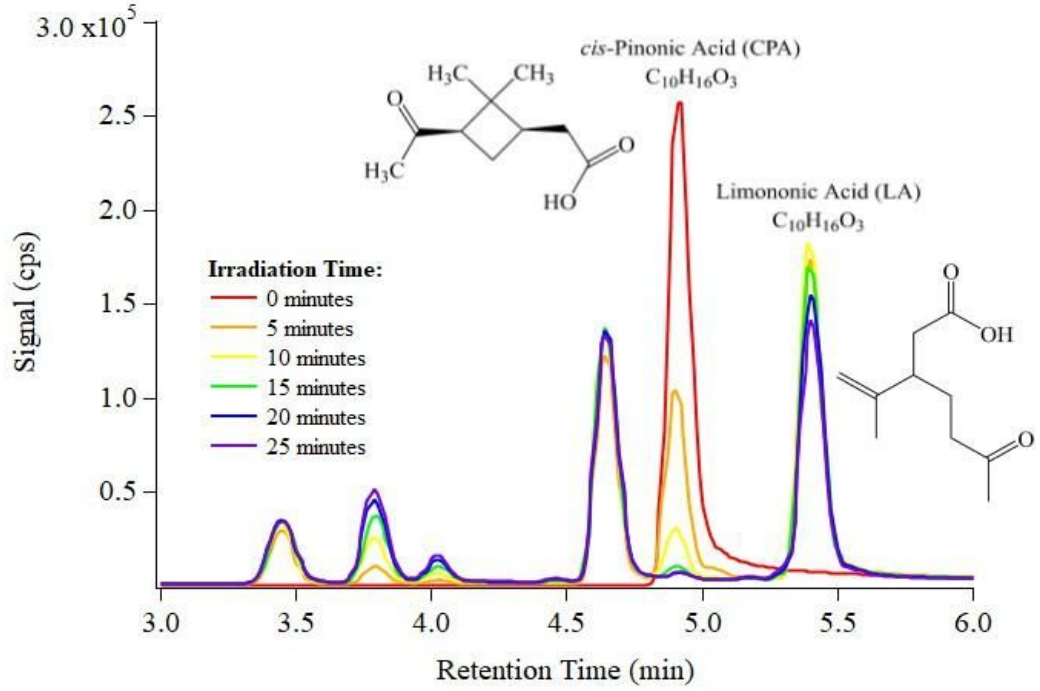

Figure S3. (-)ESI-LC/MS selected ion monitoring (SIM) chromatogram of m/z =183.1 Th (corresponding to both CPA and LA) under direct photolysis. Color coding indicates irradiation time.

As shown in Figure S3, CPA in solution is completely reacted away after 25 minutes under UVB light. Although the direct photolysis of CPA leads to the formation of more than one isomer (m/z =183.1 Th),[3,4] we can identify LA as being the peak on the far right by following Witkowski et al.[5]

Section S2. SOA Generation and Collection

A flow tube reactor was used to generate α-Pinene SOA (Figure S4). Under ambient light and in the absence of nitrogen oxides, α-Pinene and O_3 react in the flow tube to generate SOA at room temperature. No OH scavenger was added; therefore, α-pinene was oxidized primarily by O_3 but also partially by the OH radical. The flow tube reactor was operated under steady state of gas flowing at 2.0 lpm, leading to an average residence time of 2.0 min. The relative humidity (RH) in the flow tube reactor was less than 3%. No seed aerosol is used during SOA generation. An initial test confirmed that the presence of ammonium sulfate seed aerosol did not change the chemical composition of SOA collected using the flow tube reactor. SOA samples were collected on Millipore filters (0.7 μm pore size, hydrophilic glass fiber, 47 mm diameter) for 24 h and immediately frozen at -16 °C. One filter sample was collected per experiment, having an average SOA mass of 1.5-2.5 mg.

Prior to performing the experiments, the frozen SOA samples were thawed and extracted in 15 mL of Milli-Q water (18.0 mΩ) by stirring it with a magnetic bar for 5 minutes. The solution was then filtered using a Millipore Millex-FH Syringe Filter unit (0.45 μm pore size, hydrophobic PTFE, 50 mm diameter). Aqueous SOA samples were thawed, extracted and analyzed in the same day.

The chemical composition of collected SOA was analyzed by the (-)ESI-LC/MS method described in Section S4. A total ion chromatogram, along with species investigated in this work, is shown in Figure S5.

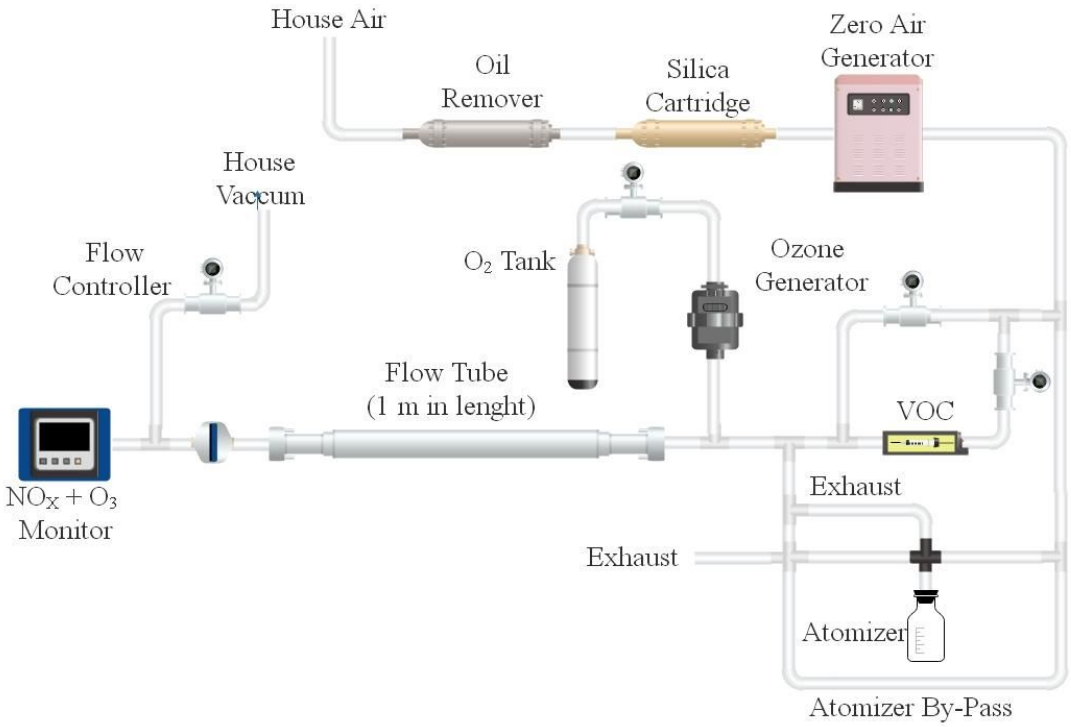

65

66 **Figure S4.** Experimental apparatus to generate and collect SOA.

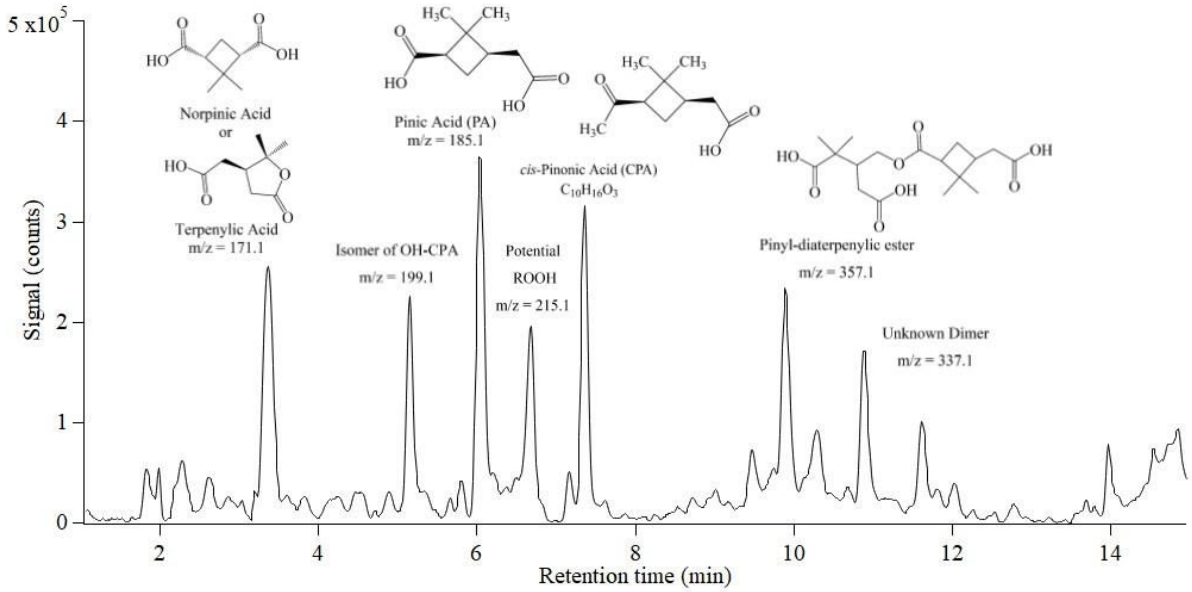

67

68 **Figure S5.** Base peak intensity (BPI) chromatogram of α-pinene SOA obtained using (-)ESI-

69 LC/MS under scanning acquisition mode (m/z = 100-500 Th; 0.95 seconds/cycle).

Section S3. Photo-Oxidation Experimental Conditions

Table S1 summarizes the concentrations of OAs, H_2O_2, and reference compounds used in photo-oxidation experiments.

Table S1. Experimental conditions for the photo-oxidation experiments.

	***cis*-Pinonic Acid (CPA)**	**Pinic Acid (PA)**	**Limononic Acid (LA)**	**WSOC of SOA**	**Formic Acid (FA)**
[Organic Acid]	30 μM	30 μM	-[a]	-[a]	2.6 mM
[Pimelic Acid]$_{Ref}$	0.3 μM	0.3 μM	0.3 μM	1.0 μM	5.0 μM
[Caffeine]$_{Ref}$	0.3 μM	3.0 μM	1.5 μM	1.0 μM	3.0 μM
[H_2O_2]	10 mM	10 mM	10 mM	30.0 mM	150 mM

[a] Concentration is not determined.

For each target compound and WSOC, control experiments were conducted by performing the experiment with no addition of H_2O_2 as the OH source. Each OA was analyzed in triplicate under uncontrolled pH, pH 2 and 10, and the results are discussed in the main article.

The OAs present in the water-soluble fraction of α-pinene ozonolysis SOA were also submitted to control experiments. For compounds that undergo direct photolysis, the direct photolysis rates were taken into consideration when calculating their respective bimolecular rate constants.

Section S4. Chemical Analysis

S4.1 ESI-LC/MS Analysis

ESI-LC/MS analyses were carried out using a reverse phase Kinetex (Phenomenex) Polar C18 column (50 x 2.1 mm, 2.6 μm, 100 Å) kept at 35.0 °C and equipped with a security guard

cartridge with a 2.1 mm ID C18 pre-column. For the investigation of individual OAs, eluent A was formic acid solution in water (pH = 2.8) and eluent B was acetonitrile (ACN), delivered at a flow rate of 0.5 mL/min; the injection volume was 15 μL. For the experiments involving the OAs present in water-soluble fraction of α-Pinene SOA, methanol (MeOH) was used as eluent B. The ESI conditions were as follows: capillary voltage was - 4.5 and + 5.5 kV in the negative and positive ionization modes. ESI in positive mode ((+)-ESI) was used to detect caffeine at pH 10 conditions. The gradient elution programs for the reactions of individual OAs were different from those in the α-pinene SOA:

Gradient Elution Program for PA, CPA and LA. 0.0−0.5 min isocratic 5% B, 0.5−5.0 min linear gradient to 30% B, 5.0−6.0 min linear gradient to 95% B, 6.0−6.7 min isocratic 95% B, 6.7− 7.0 min linear gradient to 5% B. Afterward, the column was re-equilibrated at 5% and the analysis was complete in 11.5 min.

Gradient Elution Program for the α-Pinene SOA Analysis. 0.0−1.0 min isocratic 1%, 1.0−6.0 min linear gradient to 35%, 6.0−11.0 min linear gradient to 50% B, 11.0−12.5 min linear gradient to 95% B, 12.5− 14.5 min isocratic 95% B, 14.5−15.0 min linear gradient to 1% B. Afterward, the column was re-equilibrated at 1% and the analysis was complete in 19.0 min.

S4.2 IC Analysis of Formic Acid

A Dionex ICS 5000+ chromatograph (Thermo Scientific) was used for the analysis of FA at pH 2 and pH 10. Separation was achieved using a Dionex IonPac® AS18 (4 x 150 mm) anion exchange column with a Dionex IonPac® AG18 guard column (4 x 30 mm). The eluent was potassium hydroxide (KOH) run at a flow rate of 1.0 mL/min. The gradient method held 12 mM KOH for one minute, then increased to 30 mM KOH from 1 to 14 min, then held 44 mM KOH

from 14 to 15 min, then equilibrated at 12 mM KOH from 15 to 18 min, for a total run time of 18 minutes. Formate standards at concentrations of 0.25, 0.50, 0.75, 1.0 and 2.5 ppm were made from their salts for instrument calibration, and water was used as blank (0 ppm) standard. Offline LC-MS was carried out on the same day of IC analysis to monitor the decay of reference compounds over the irradiation time.

The conductivity detector on the IC system cannot tolerate SO_4^{2-} concentrations greater than 10 ppm. This posed a challenge to our pH 2 experiment, as we had to add 600 ppm of H_2SO_4 for pH adjustment. A dilution factor of 60 was required for the sample to be compatible with the IC analysis. Hence, we had to use much higher concentrations of FA and H_2O_2 to accommodate this requirement.

Section S5. Kinetic Modeling of CPA Photochemistry

S5.1 Model Description

A kinetic box model was developed to better characterize the photoreactor used in this work and to evaluate the importance of radical chemistry that cannot be tracked using our analytical methods. The kinetic box model considers aqueous-phase species and their reactions listed in Table S2. The rate coefficients were adapted from Tan et al.[6] unless otherwise noted. The kinetic scheme was executed using Matlab (Mathwork) to simulate the concentration of species as a function of irradiation time. The model simulates direct photolysis, bimolecular reactions, and acid-base chemistry of selected species.

The direct photolysis rate of a species (J) is simulated by eq. S1:

$$J = \int_{\lambda_{\min}}^{\lambda_{\max}} I(\lambda)\sigma(\lambda)\Phi(\lambda)d\lambda \approx \sum_{\lambda} I(\lambda)\sigma(\lambda)\Phi(\lambda)\Delta\lambda \quad \text{, eq. S1}$$

where $I(\lambda)$, $\sigma(\lambda)$, and $\Phi(\lambda)$ are the light flux, molecular absorption cross section, and quantum yield, respectively. While $\sigma(\lambda)$ and $\Phi(\lambda)$ were obtained from the literature, $I(\lambda)$ in our photoreactor was determined using a combination of direct measurement and chemical actinometry. First, the emission spectra of the UVB lamps were recorded using a spectroradiometer (Ocean Optics, USB2000+ER). Second, 2-nitrobenzaldehyde (2-NB) was employed as a chemical actinometer to quantify the absolute amount of light reaching molecules inside the aqueous solution. Briefly, the photolysis rate of 2-NB in the photoreactor was monitored using high performance liquid chromatography (HPLC).[7] Spectra recorded by the spectroradiometer was then scaled until it matched the photon flux needed to achieve the observed 2-NB photolysis rate. Figure S6 below presents the photon flux determined using this method.

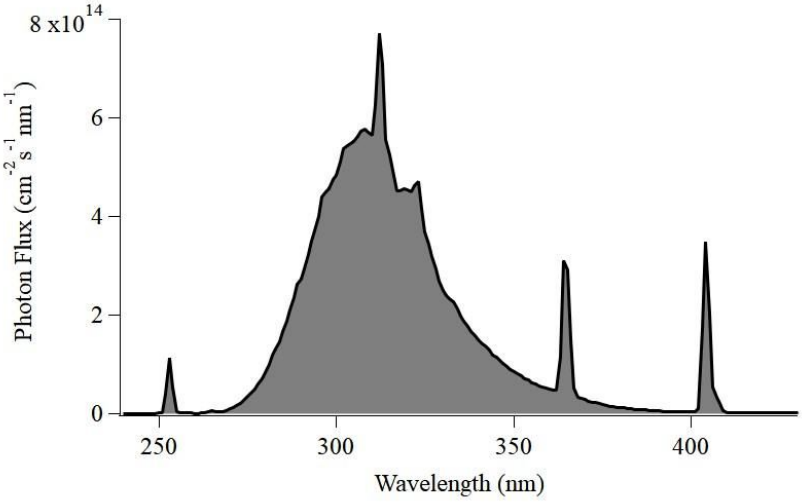

Figure S6. Photon flux spectrum of the photoreactor.

In the CPA photochemistry model, the J values of two species are simulated: H_2O_2 and CPA. The $\sigma(\lambda)$, and $\Phi(\lambda)$ of these two compounds were referred from Finlayson-Pitts and Pitts[8] and Lignell et al.,[3] respectively. The effective OH radical yield (Φ_{OH}) of H_2O_2 photolysis in the aqueous phase is smaller than that in the gas phase due to the solvent cage effect. Therefore, an effective $\Phi_{OH} = 0.93$ suggested by Herrmann et al.[9] is applied.

Direct photolysis and OH-oxidation of CPA result in numerous products and describing an explicit oxidation mechanism in the model is implausible. Given that the major purpose of the model is to simulate the decay of CPA, the products of CPA are lumped into a single category "CPAprod". CPA contains a four-membered ring on its structure, and the 1st-generation products of CPA (by both photolysis and OH-oxidation) are likely those arising from ring-opening reaction and functionalization reactions. The 2nd and subsequent oxidation will, however, result in either fragmentation or functionalization reactions. The probability of fragmentation (P_{frag}) is an ongoing focus of research. Cappa and Wilson[10] parameterized P_{frag} using eq. S2:

$$P_{\mathrm{frag}} = c_{\mathrm{frag}} \times N_{\mathrm{O}} \quad , \qquad \text{eq. S2}$$

where c_{frag} is a fitting parameter, and N_O is the number of oxygens on the molecule. The authors found that $c_{frag} = 0.18$ best reproduced α-pinene SOA formation in chamber experiments. CPA has $N_O = 3$, its products (CPAprod) will likely contain N_O of 3, 4, or 5. Therefore, P_{frag} for CPA oxidation is estimated to be between 0.58 and 0.9. In this model, we took the value of $P_{frag} = 0.7$ as an estimated value of all the CPAprod species.

The k^{II}_{OH} values of CPAprod species can be either faster or slower than CPA itself, depending on their structures. In this model, we assumed that all the products react with OH with the same k^{II}_{OH} to CPA. This assumption is reasonable if the products contain similar numbers of carbon in their

structures (i.e., for early-generation products). However, uncertainty cumulates towards products arising in the later generations.

Table S2. Reactions and Rate Coefficients Used in the CPA Photochemical Model.

Reactions	Rate Coefficient [a]	Ref. [b]	Footnote
$H_2O_2 + h\nu \rightarrow 2OH$	-		c
$HO_2 + HO_2 \rightarrow H_2O_2 + O_2$	8.3×10^5		
$OH + H_2O_2 \rightarrow HO_2 + H_2O$	2.7×10^7		
$HO_2 + H_2O_2 \rightarrow OH + O_2 + H_2O$	3.7		
$OH + HO_2 \rightarrow O_2 + H_2O$	7.1×10^9		
$H_2O \rightarrow H^+ + OH^-$	1.4×10^{-3} s^{-1}		
$H^+ + OH^- \rightarrow H_2O$	1.4×10^{11}		
$H_2O_2 \rightarrow H^+ + HO_2^-$	0.35 s^{-1}	11	
$H^+ + HO_2^- \rightarrow H_2O_2$	2.3×10^{-10}		
$OH \rightarrow H^+ + O^-$	0.18 s^{-1}		
$H^+ + O^- \rightarrow OH$	2.3×10^{-10}		
$HO_2 \rightarrow H^+ + O_2^-$	8.0×10^5 s^{-1}		
$H^+ + O_2^- \rightarrow HO_2$	5.0×10^{10}		
$CO_2^- + O_2 \rightarrow O_2^- + CO_2$	2.4×10^9		
$OH + O_2^- \rightarrow OH^- + O_2$	1.0×10^{10}		
$HCO_3^- + OH \rightarrow CO_3^- + H_2O$	1.0×10^7		
$CO_3^- + O_2^- \rightarrow CO_3^{2-} + O_2$	6.5×10^8		
$CO_3^- + H_2O_2 \rightarrow HCO_3^- + HO_2$	8.0×10^5		
$CO_2 \rightarrow H^+ + HCO_3^-$	2.4×10^{-2} s^{-1}		

$H^+ + HCO_3^- \rightarrow CO_2$	5.6×10^4		
$HCO_3^- \rightarrow H^+ + CO_3^{2-}$	$2.3\ s^{-1}$		
$H^+ + CO_3^{2-} \rightarrow HCO_3^-$	5.0×10^{10}		
CPA + hν → CPAprod	-	3	
CPA + OH → CPAprod	Experimental values		d
CPAprod + OH → CPAprod (30%) → 2CPAprod (70%)	Experimental values		d
PMA + OH → PMAprod	2.2×10^9 (pH 2) 3.4×10^9 (pH 4)	12	
PMAprod + OH → PMAprod (30%) → 2PMAprod (70%)	2.2×10^9 (pH 2) 3.4×10^9 (pH 4)		
CAF + OH → CAFprod	6.9×10^9	4	
CAFprod + OH → CAFprod (30%) → 2CAFprod (70%)	6.9×10^9		

The following reactions are used only in the SO_4^- scenario

$HSO_4^- \rightarrow H^+ + SO_4^{2-}$	$5.2 \times 10^8\ s^{-1}$	13
$H^+ + SO_4^{2-} \rightarrow HSO_4^-$	5.0×10^{10}	13
$HSO_4^- + OH \rightarrow SO_4^- + H2O$	3.5×10^5	14
$SO_4^- + SO_4^- \rightarrow S_2O_8^{2-}$	2.6×10^{-13}	15
$SO_4^- + H_2O_2 \rightarrow SO_4^{2-} + HO_2$	4.6×10^{-14}	
$SO_4^- + HO_2 \rightarrow SO_4^{2-} + H^+ + O_2$	5.8×10^{-12}	
$SO_4^- + O_2^- \rightarrow SO_4^{2-} + O_2$	5.8×10^{-12}	
$SO_4^- + OH^- \rightarrow SO_4^{2-} + OH$	2.3×10^{-14}	

$SO_4^- \rightarrow H^+ + OH + SO_4^{2-}$	5.0×10^2 s^{-1}	16	
$SO_4^- + S_2O_8^{2-} \rightarrow SO_4^{2-} + S_2O_8^-$	1.0×10^{-15}	17	
CPA + $SO_4^- \rightarrow$ CPAprod	Experimental values		e
PMA + $SO_4^- \rightarrow$ PMAprod	2.2×10^9 (pH 2) 3.4×10^9 (pH4)		e

Acronyms: CPA: *cis*-pinonic acid, PMA: pimelic acid, CAF: caffeine, prod: products of a species

[a] Unit of rate coefficients is M^{-1} s^{-1} unless otherwise noted.

[b] Rate coefficients are adapted from Tan et al.[6] unless otherwise noted.

[c] Consideration for $\Phi_{OH} = 0.93$ is applied.[9]

[d] Experimentally determined k^{II}_{OH} values were used for pH 2, 4 (uncontrolled), and 10.

[e] Reactivity of SO_4^- is assumed to be the same as the OH reactivity.

S5.2 Model Scenarios

The initial concentrations used for all the model scenarios are shown in Table S3 below.

Reproducing Experimental Results

The model was first operated to reproduce experimental results of CPA direct photolysis and OH-oxidation. For CPA direct photolysis, the H_2O_2 concentration was prescribed to be 0. Given that direct photolysis rate of CPA was not dependent on pH, we simulated only a single pH condition (pH 4). For CPA OH-oxidation experiments, the H_2O_2 initial concentration was set to match that used in the experiment, and the subsequent radical chemistry is simulated in the model. The initial pH value was set to be 2, 4, and 10, where pH 4 was used to represent

experiments conducted under uncontrolled pH. The experimentally determined k^{II}_{OH} values of CPA (see main text) under each pH condition were employed in these simulations. The reference compounds, pimelic acid (PMA) for acidic conditions and caffeine (CAF) for pH 10, were also considered in the simulations.

Impact of pH

To evaluate whether an altering pH will affect the steady-state OH concentration ($[OH]_{ss}$), and hence affect the decay rate of CPA, a case study was conducted to investigate potential impact of pH. In this case, the reactivity of CPA was prescribed to be a fixed value (2.9×10^9 M^{-1} s^{-1}) across the entire pH range. The initial concentration was set to be pH 2, 4, and 10 for the simulations. The reference compounds and their chemistry were excluded from this case.

Potential Impact of Sulfate Radical Formation

Studies from the past years have observed formation of organo-sulfate compounds under irradiated conditions,[18,19] presumably due to chemistry of sulfate radicals (SO_4^-) and bisulfate radicals (HSO_4). In our pH 2 experiments, H_2SO_4 was added to the solution for pH adjustment. A case study was conducted to explore whether SO_4^- can form and affect the decay of CPA at pH 2 using rate coefficients available on the literature.[15] It is assumed that the only formation mechanism of SO4$^-$ is from OH + bisulfate anion (HSO_4^-), with the rate coefficient provided in McNeil et al.[14] The rate coefficient of SO_4^- + CPA has not been reported. We assumed that SO_4^- reacts with CPA as rapidly as OH reacting with CPA (i.e., $k^{II}_{SO4} = 2.9\times 10^9$ M^{-1} s^{-1}). We note that this is an upper-band estimate for the impact of SO_4^-, as previous studies have shown that the reactivity of SO_4^- can be much smaller than that of OH, at times by a factor of 50 to 100.[15] Another aspect of SO_4^- that is of great interest is its ability to regenerate OH radical through

reactions with H_2O and OH^-. The rate coefficient of this reaction has been reported by Hermann et al.[16]

Table S3. Initial Concentrations Used in Model Scenarios.

Scenarios	CPA (μM)	H_2O_2 (mM)	Ref. Cmpd (μM)	pH	SO_4^- chemistry
Simulating Experimental Results					
CPA direct photolysis	30	0	0	4	No
CPA OH-oxidation	30	10	0.3	2,4,10	No
Investigating the Impact of pH					
CPA OH-oxidation	30	10	0	2,4,10	No
Investigating the Impact of SO_4^-					
CPA OH-oxidation	30	10	0.3	2	Yes

S5.3 Model Results

Reproducing Experimental Results

Model results simulating the experiments are shown in Figure S7. For direct photolysis of CPA (Figure S7a), the model underestimated the decay of CPA when a quantum yield of 0.5, reported by Lignell et al.,[3] was used. An adjustment of the quantum yield to 0.69 resulted in the best model-observation agreement in terms of the pseudo-1st order decay rate of CPA. Therefore, we have used this adjusted quantum yield for all the rest of the simulations. The model-observation agreement for CPA OH-oxidation was generally reasonable.

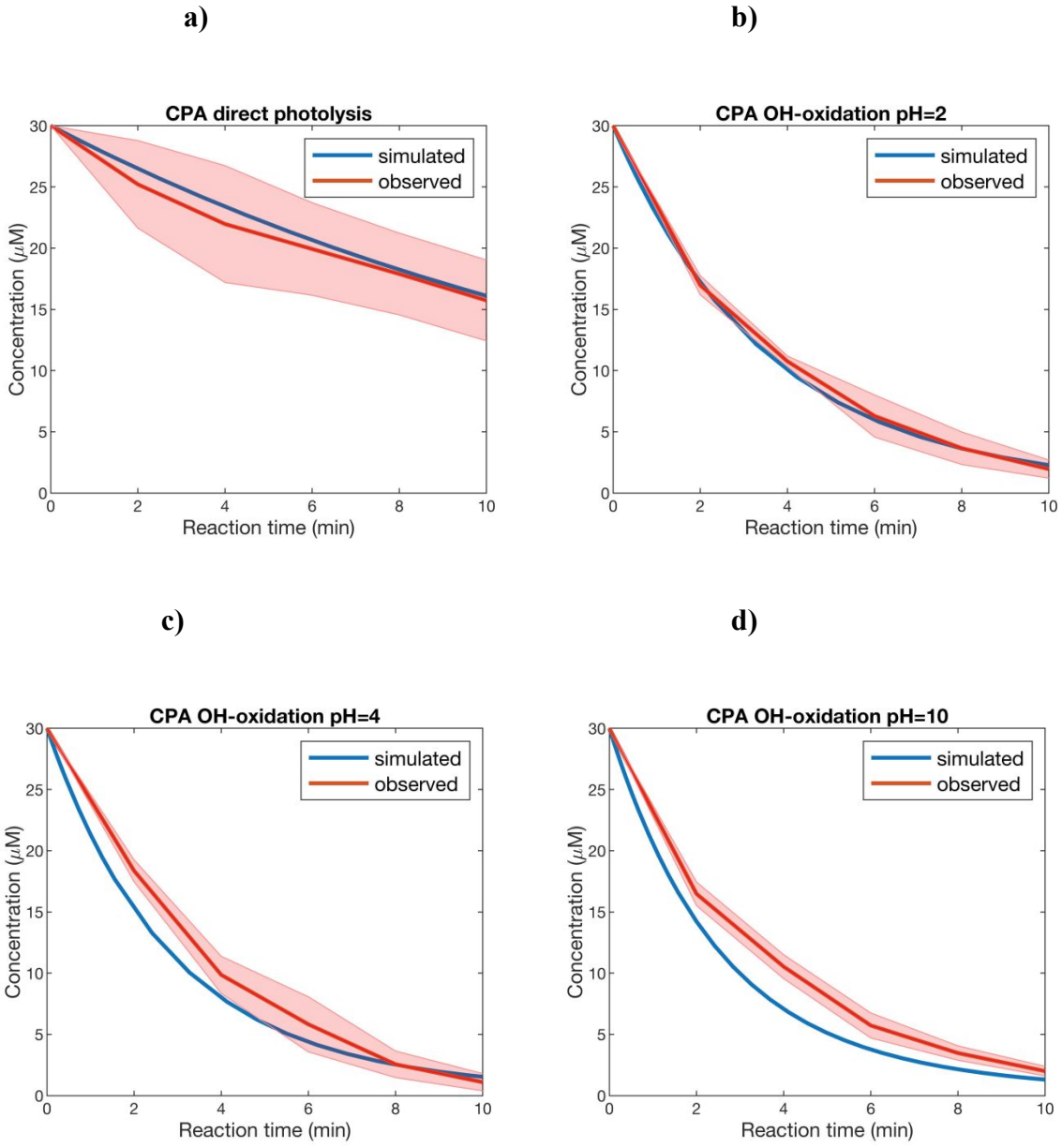

Figure S7. Simulated and observed CPA concentration in a) direct photolysis, b) OH-oxidation at pH 2, c) OH-oxidation at pH 4, and d) OH-oxidation at pH 10. The shaded area presents observed data standard deviation range (1 σ). The model result in a) employs the optimized CPA Φ(λ) value: 0.69 across the relevant wavelength rage.

Impact of pH Conditions

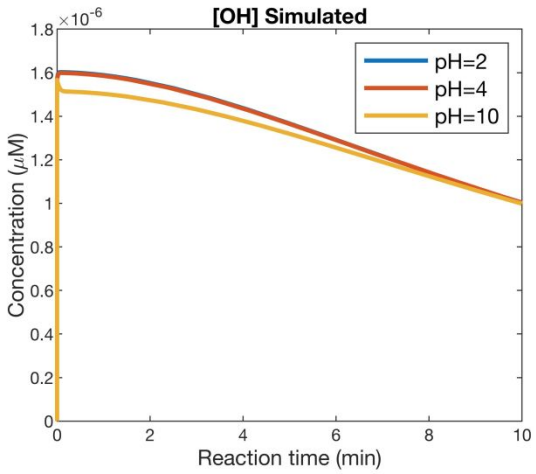

Figure S8. OH concentrations simulated at pH 2, 4, and 10.

Impact of SO_4^-

a) **b)**

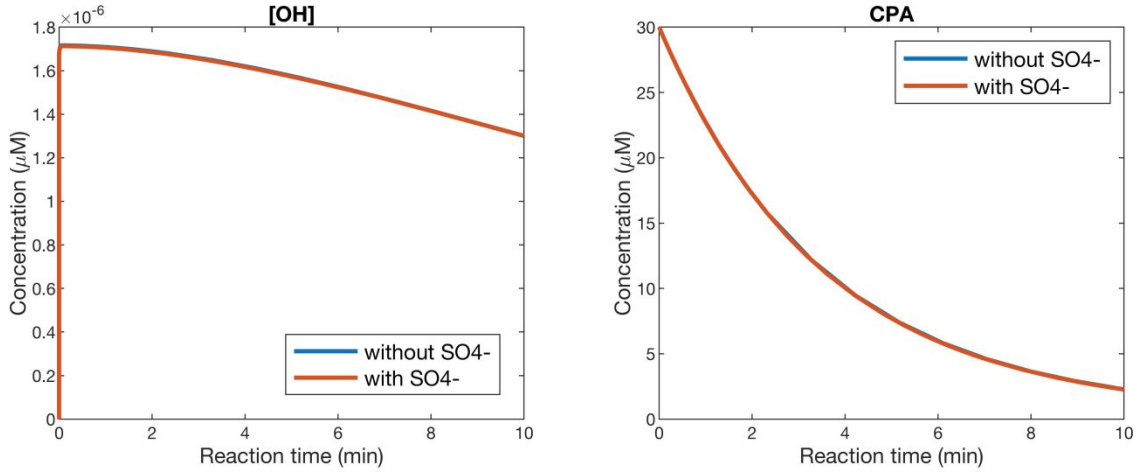

Figure S9. The simulated a) [OH] and b) CPA concentration with and without the SO_4^- chemistry included in the model.

Section S6. Additional Experimental Data

S6.1 OH-Reactivities of CPA and LA

Figure S10 shows a (-)ESI-LC/MS chromatogram obtained under SIM acquisition mode for a typical CPA OH-oxidation experiment under uncontrolled pH and Figure S11 shows a compilation of (-)ESI- and (+) ESI-LC/MS SIM chromatogram for a typical LA photo-oxidation experiment at pH 10. The color scheme represents the irradiation time during the photo-oxidation experiment.

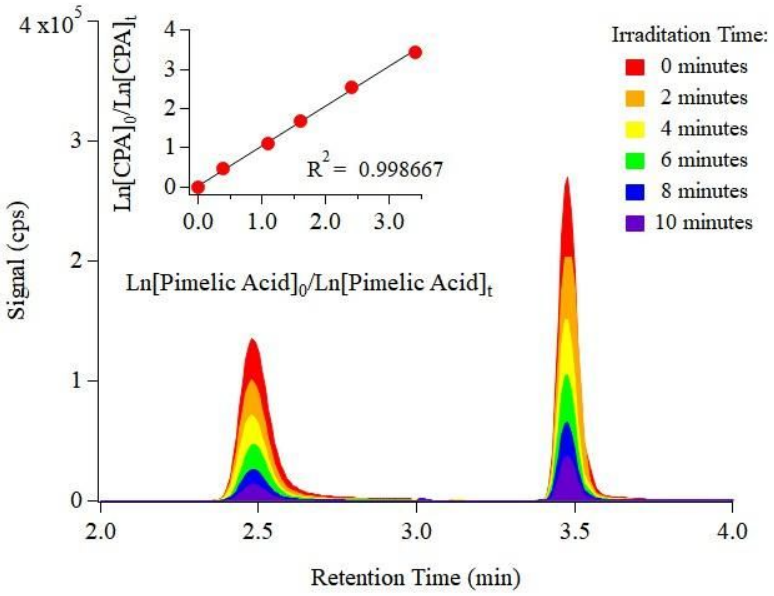

Figure S10. SIM chromatogram of CPA (m/z = 183.1 Th) and pimelic acid (reference compound, m/z = 159.1 Th) under 10 min of UVB irradiation.

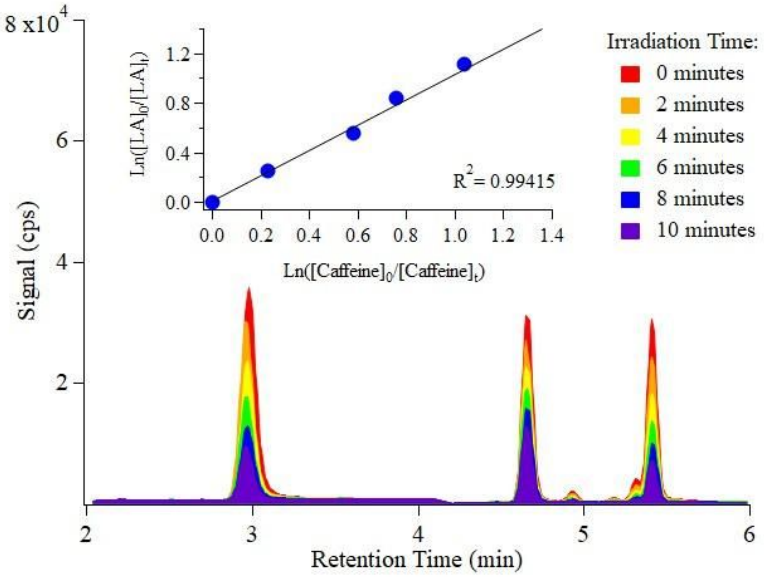

Figure S11. SIM chromatogram of LA (m/z = 183.1 Th) and caffeine (reference compound, m/z = 195.1 Th) under 10 min of UVB irradiation. LA peak is the one most retained (longer retention time) in the chromatogram.

S6.2 Bimolecular Rate Coefficients of SOA Water Soluble Organic Compounds (WSOCs) Targeted

Table S4. Bimolecular rate coefficient for α-pinene SOA WSOC's reactions with OH radicals (k^{II}_{OH} in $M^{-1}\ s^{-1}$).

		pH 2	Uncontrolled pH	pH 10
Norpinic or Terpenylic Acid	m/z = 171.1	$(2.0 \pm 0.2) \times 10^8$	$(2.9 \pm 0.4) \times 10^8$	$(6.4 \pm 0.9) \times 10^8$
Pinic Acid	m/z = 185.1	$(1.6 \pm 0.0) \times 10^9$	$(2.2 \pm 0.1) \times 10^9$	$(2.4 \pm 0.3) \times 10^9$
Potential Peroxide	m/z = 215.1	$(8.2 \pm 0.1) \times 10^8$	$(1.3 \pm 0.1) \times 10^9$	$(1.9 \pm 0.0) \times 10^9$
cis-Pinonic Acid	m/z = 183.1	$(2.2 \pm 0.3) \times 10^9$	$(3.4 \pm 0.1) \times 10^9$	$(3.3 \pm 0.3) \times 10^9$
Pinyl-diaterpenylic Ester	m/z = 357.1	$(2.1 \pm 0.1) \times 10^9$	$(3.2 \pm 0.6) \times 10^9$	$(3.2 \pm 0.4) \times 10^9$
Isomer of OH-CPA	m/z = 199.1	$(3.1 \pm 0.0) \times 10^9$	$(4.7 \pm 0.0) \times 10^9$	$(4.8 \pm 0.1) \times 10^9$

References

(1) Steimer, S. S.; Delvaux, A.; Campbell, S. J.; Gallimore, P. J.; Grice, P.; Howe, D. J.; Pitton, D.; Claeys, M.; Hoffmann, T.; Kalberer, M. Synthesis and Characterisation of Peroxypinic Acids as Proxies for Highly Oxygenated Molecules (HOMs) in Secondary Organic Aerosol. *Atmos. Chem. Phys.* **2018**, *18* (15), 10973–10983.

(2) Schrader, W.; Geiger, J.; Godejohann, M. Studies of Complex Reactions Using Modern Hyphenated Methods: α-Pinene Ozonolysis as a Model Reaction. *J. Chromatogr. A* **2005**, *1075* (1), 185–196.

(3) Lignell, H.; Epstein, S. A.; Marvin, M. R.; Shemesh, D.; Gerber, B.; Nizkorodov, S. Experimental and Theoretical Study of Aqueous Cis-Pinonic Acid Photolysis. *J. Phys. Chem. A* **2013**, *117* (48), 12930–12945.

(4) Witkowski, B.; Gierczak, T. Cis-Pinonic Acid Oxidation by Hydroxyl Radicals in the Aqueous Phase under Acidic and Basic Conditions: Kinetics and Mechanism. *Environ. Sci. Technol.* **2017**, *51* (17), 9765–9773.

(5) Witkowski, B.; Jurdana, S.; Gierczak, T. Limononic Acid Oxidation by Hydroxyl Radicals and Ozone in the Aqueous Phase. *Environ. Sci. Technol.* **2018**, *52* (6), 3402–3411.

(6) Tan, Y.; Perri, M. J.; Seitzinger, S. P.; Turpin, B. J. Effects of Precursor Concentration and Acidic Sulfate in Aqueous Glyoxal−OH Radical Oxidation and Implications for Secondary Organic Aerosol. *Environ. Sci. Technol.* **2009**, *43* (21), 8105–8112.

(7) Galbavy, E. S.; Ram, K.; Anastasio, C. 2-Nitrobenzaldehyde as a Chemical Actinometer for Solution and Ice Photochemistry. *J. Photochem. Photobiol. Chem.* **2010**, *209* (2), 186–192.

(8) Finlayson-Pitts, B. J.; Pitts Jr, J. N. *Chemistry of the Upper and Lower Atmosphere: Theory, Experiments, and Applications*; Academic press, 1999.

(9) Herrmann, H.; Hoffmann, D.; Schaefer, T.; Braeuer, P.; Tilgner, A. Tropospheric Aqueous-Phase Free-Radical Chemistry: Radical Sources, Spectra, Reaction Kinetics and Prediction Tools. *Chem. Phys. Chem.* **2010**, *11* (18), 3796–3822.

(10) Cappa, C. D.; Wilson, K. R. Multi-Generation Gas-Phase Oxidation, Equilibrium Partitioning, and the Formation and Evolution of Secondary Organic Aerosol. *Atmos. Chem. Phys.* **2012**, *12* (20), 9505–9528.

(11) Zhang, Y.; Xiao, Y.; Zhang, J.; Chang, V. W. C.; Lim, T.-T. Degradation of Cyclophosphamide and 5-Fluorouracil in Water Using UV and UV/H2O2: Kinetics Investigation, Pathways and Energetic Analysis. *J. Environ. Chem. Eng.* **2017**, *5* (1), 1133–1139.

(12) Schaefer, T.; Wen, L.; Estelmann, A.; Maak, J.; Herrmann, H. PH- and Temperature-Dependent Kinetics of the Oxidation Reactions of OH with Succinic and Pimelic Acid in Aqueous Solution. *Atmosphere* **2020**, *11* (4), 320.

(13) Lim, H.-J.; Carlton, A. G.; Turpin, B. J. Isoprene Forms Secondary Organic Aerosol through Cloud Processing: Model Simulations. *Environ. Sci. Technol.* **2005**, *39* (12), 4441–4446.

(14) McNeill, V. F.; Woo, J. L.; Kim, D. D.; Schwier, A. N.; Wannell, N. J.; Sumner, A. J.; Barakat, J. M. Aqueous-Phase Secondary Organic Aerosol and Organosulfate Formation in Atmospheric Aerosols: A Modeling Study. *Environ. Sci. Technol.* **2012**, *46* (15), 8075–8081.

(15) Herrmann, H.; Ervens, B.; Jacobi, H.-W.; Wolke, R.; Nowacki, P.; Zellner, R. CAPRAM2.3: A Chemical Aqueous Phase Radical Mechanism for Tropospheric Chemistry. *J. Atmos. Chem.* **2000**, *36* (3), 231–284.

(16) Herrmann, H. On the Photolysis of Simple Anions and Neutral Molecules as Sources of O−/OH, SOx− and Cl in Aqueous Solution. *Phys. Chem. Chem. Phys.* **2007**, *9* (30), 3935–3964.

(17) Herrmann, H.; Reese, A.; Zellner, R. Time-Resolved UV/VIS Diode Array Absorption Spectroscopy of SOx−(X=3, 4, 5) Radical Anions in Aqueous Solution. *J. Mol. Struct.* **1995**, *348*, 183–186.

(18) Altieri, K. E.; Seitzinger, S. P.; Carlton, A. G.; Turpin, B. J.; Klein, G. C.; Marshall, A. G. Oligomers Formed through In-Cloud Methylglyoxal Reactions: Chemical Composition, Properties, and Mechanisms Investigated by Ultra-High Resolution FT-ICR Mass Spectrometry. *Atmos. Environ.* **2008**, *42*

(19) Nozière, B.; Ekström, S.; Alsberg, T.; Holmström, S. Radical-Initiated Formation of Organosulfates and Surfactants in Atmospheric Aerosols. *Geophys. Res. Lett.* **2010**, *37* (5).